

Three Dimensional Modelling of MISFET

Preetam Jain, Lochan Jolly

ME Student

Department of Electronics & Telecommunication, TCET Mumbai

Professor Department of Electronics & Telecommunication, TCET Mumbai

Abstract—

Recent research shows the tremendous potential for the development of optical devices viz. photo-detector, optical sources, connectors and applications etc. This is mainly because of the success of optical communication in the recent for gigabit transmission and is intended for terabits transmission in future. In this paper, mathematical model for the optical dependence of I-V, C-V characteristics of MISFET structure (to be used as photo-detector) is reported. Model is based on solution of Poisson's and current continuity equation. Proposed structure of MISFET includes, $\text{In}_{0.53}\text{Ga}_{0.47}\text{As}$ used as substrate material and InP as insulator. Light is made to incident perpendicular to the surface. Drain current can be controlled optically by means of varying light intensity of incident radiation. There is significant effect of intensity modulation on IV and CV characteristics of MISFET. As a result of intensity modulation, drain current increases significantly in presence of illumination mainly due to change in carrier concentration of channel results from photo-generated carriers. Simulation of mathematical model is carried out in MATLAB.

Keywords—MISFET; Modeling; Optical

I. INTRODUCTION

Ever since ancient times, people had a principle need to communicate with one another. This need created interests in devising communication system for sending messages from one distant place to another. Optical communication methods were of special interest among the many systems. The basic function of an optical fiber link is to transport a signal from communication equipment at one location to corresponding equipment at another location with a high degree of reliability and accuracy. The main constituents of an optical fiber communication link are transmitter consisting of optical source, an optical cable and a receiver consisting of a photo-detector. Photo-detector is the first element of the photo receiver circuit which interprets the information contained in the optical signal. They demodulate the optical signal that are subsequently amplified and processed to obtain the actual information signal. For such applications, photo-detectors must have high sensitivity, high responsivity and minimum noise. In addition, the photo-detectors should be compact in size, use low biasing voltage and current, reliable under operating condition, and preferably integrated circuit compatible [1,2].

Field effect transistors (FET) devices are sensitive to light, having high package density and are suitable for microwave applications. Lots of efforts are carried out in the development of microwave transistors from III-V compound semiconductor material systems [4]. Presently the GaAs Schottky-gate FET (MESFET) is the only such device commercially available. Irrespective of remarkable

microwave gain and noise performance, this device suffers from the limitations of a restricted range of enhancement operations. Schottky contact gate structure of GaAs MESFET produces large gate leakage current, when used on InP and InGaAs. MIS structure offers very low leakage current and reduces gate capacitances. $\text{In}_x\text{Ga}_{1-x}\text{As}$ is a promising material for advanced optoelectronic devices. $\text{In}_{0.53}\text{Ga}_{0.47}\text{As}$ is a good substrate for such circuits. $\text{In}_{0.53}\text{Ga}_{0.47}\text{As}$ lattice matched to semi-insulating InP has higher low field mobility, high drift mobility and peak electron velocity [5,6]. Therefore, InGaAs MISFETs have potential for better microwave performance.

In the paper an optically gated Metal-Insulator-Semi conductor Field-Effect-Transistor (MISFET) structure has been characterized theoretically to examine its potential as an photo-detector in 1 to 1.6 μm wavelength region. Numerical calculations have been carried out to determine the I-V characteristics of the device in various illuminated conditions. Quantum efficiency of MISFET is also calculated.

II. THEORY

The schematic structure of the MISFET under consideration is shown in fig.1 for the case of a n-channel formed on a p-type substrate. The n^+ source and drain regions can be formed by using ion-implantation into the relatively lightly doped p-type substrate. A thin semi-insulating InP (InP:Fe) layer separates the semi-transparent metal gate from the InGaAs surface. The thickness of the device is considered along the x-axis, length along the y-axis and width along the z-axis. The optical radiation is incident in the x-direction and drain to source current flows in y direction. The doping concentration of p-

InP has been assumed to be $10^{21}/\text{m}^3$. The thickness of the insulator has been assumed to be 390nm. The length and width of the device is $0.2 \mu\text{m}$ and $100 \mu\text{m}$ respectively.

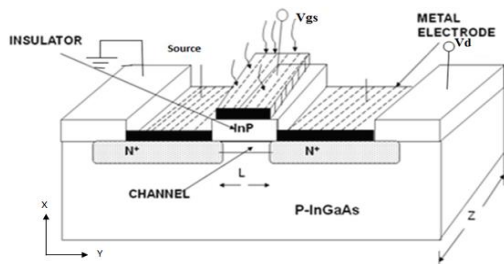


Fig. 1 Structure of InGaAs MISFET

A. Device Mechanism

In the absence of illumination, when a sufficiently large positive bias is applied to the gate so that surface inversion layer is formed between the two n^+ regions, the source and the drain are connected by a conducting n-channel surface through which a large current can flow. The conductivity of the channel can be modulated by the gate bias voltage.

When a voltage is applied across the source-drain contacts, the structure is in non-equilibrium condition and current flows from drain to source. Absorption of suitable wavelength in the semiconductor causes additional generation of electron-hole pairs. The hole move towards the bulk while the electrons accumulate near the surface causing a change in the conductivity of the surface channel. The excess photo generated carriers also cause a change in the minority carrier lifetime. The overall effect is a net increase in drain current under illumination in the steady-state for a particular drain to source voltage.

The change in the conductivity of the surface channel under the illumination however, depends on the value of incident optical power. It is thus possible to vary the conductivity of the channel by changing the incident optical power without changing the gate bias voltage. This particular feature of the device enables one to use it as an optical detector and / or optically controlled amplifier.

III. MODELING OF THE DEVICE

A. Calculation of Photovoltage

The optical radiation has been assumed incident in the vertical x-direction P_{opt} , the total photo-generation, G_{op} in the gate depletion region can be obtained as

$$G_{op}(y) = \frac{P_{opt}}{hY} (1 - R_m)(1 - R_i)(1 - R_s) \int_0^1 \int_0^{y_{dg}(x)} \alpha e^{-\alpha y} dy dx \quad (1)$$

The upper limit $y_{dg}(x)$ depends on the channel voltage and, thus, also on channel length,

$$y_{dg} = \text{sqr}t\left(\frac{2\epsilon}{N_d}(\Phi_B - \Delta + v(x) - V_{gs})\right) \quad (2)$$

In the presence of a large gate bias resistance, the photo-voltage developed at the Schottky contact can be approximated by the open-circuit voltage, given by

$$V_{op} = \frac{KT}{q} \ln \frac{J_p}{J_s} = \frac{KT}{q} \ln \left(\frac{qv_y p(0)}{J_{s1}} \right) \quad (3)$$

Where, $p(0)$ is number of holes crossing the junction at $y=0$ and is given by

$$p(0) = \frac{\pi}{4} z (p_1 r_1^2 + p_2 r_2^2) \quad (4)$$

Where $p_1 = \alpha \Phi_1 \tau_{wp} e^{-\alpha r_1}$, $p_2 = \alpha \Phi_1 \tau_{wp} e^{-\alpha r_2}$

The sidewalls of the gate depletion region are assumed quarter arcs. Considering, the arcs at the source and drain ends to have radii r_1 and r_2 , respectively, where

$$r_1 = y_{dg} \text{ at } V(x)=0$$

$$r_2 = y_{dg} \text{ at } V(x)=V_d$$

J_{s1} is the minority carrier current density of the Schottky junction and is given by

$$J_{s1} = A^* T^2 \exp(-qV_{bi}/KT) \quad (5)$$

$$A^* = \frac{4\pi q K^2 m_n^*}{h^3} \quad (6)$$

ϵ Permittivity of the semiconductor

m_n^* Effective mass of the electron

K Boltzman constant

T Room Temperature

q Charge of an electron

V_{bi} Built in voltage across the n-p junction

P_{opt} Incident optical power density

h Planck's constant

V_d Drain to source voltage

$v(x)$ channel voltage

Φ_B Schottky barrier height

Δ position of Fermi level at the neutral region below the conduction band

V_{gs} gate to source voltage

N_d substrate concentration

Y is the operating frequency

α is the absorption coefficient of the semiconductor at the operating wavelength,

R_m , R_i and R_s are the reflection coefficient at the metal gate entrance, gate-insulator interface and the insulator-semiconductor interface respectively.

B. Three dimensional Poisson's equation

$$\frac{\partial^2 \psi(x, y, z)}{\partial x^2} + \frac{\partial^2 \psi(x, y, z)}{\partial y^2} + \frac{\partial^2 \psi(x, y, z)}{\partial z^2} = \frac{-q(N_d(y) + \Delta n)}{\epsilon_s} \quad (7)$$

ψ is the three dimensional potential distribution across the channel.

where $N_d(y)$ is the non uniform doping density along x direction and is given by

$$N_d(y) = \frac{Q}{\sigma\sqrt{2\pi}} \exp\left(-\frac{(y-R_p)^2}{\sigma^2}\right)$$

where Q Ion implanted dose
σ Straggle parameter
R_p Projected range

The boundary conditions are taken from [gawri] to solve equation (7). The electric fields E_x, E_y and E_z, along x, y and z direction respectively have been obtained by solving equation(7) using Leibmann's iterative method [8].

$$E_x = \frac{\Psi(i+1,j,k) - \Psi(i-1,j,k)}{2m_x} \quad (8)$$

$$E_y = \frac{\Psi(i,j+1,k) - \Psi(i,j-1,k)}{2m_y} \quad (9)$$

$$E_z = \frac{\Psi(i,j,k+1) - \Psi(i,j,k-1)}{2m_z} \quad (10)$$

These equations have been utilized for estimating the field dependent mobility and the drain current characteristics equation. The field dependent mobility is given

$$\mu_n(E_y) = \mu_0 + \frac{2(-2\epsilon_0 E_c + 3v_{sat})}{E_c^2} E_y + \frac{3(\epsilon_0 E_c - 2v_{sat})}{E_c^3} E_y^2 \quad (11)$$

where

μ₀ Low field electron mobility
V_{sat} Saturation velocity
E_c Critical field

IV. CURRENT MODELING

Optically generated voltage increases the potential across the insulator. Let V₀ is the potential across the insulator considering optical effect is given by [7],

$$V_0 = \frac{Q_s}{C_i} \text{ and } V_0 = V_{gsop} - \Psi_s \quad (12)$$

where V_{gsop} = (V_{gs} + V_{op})

Total induced charge in the semiconductor per unit area Q_s, under illumination is given by,

$$Q_s = (V_0 \cdot C_i) = (V_{gsop} - \Psi_s) C_i \quad (13)$$

Where Ψ_s is the surface potential

C_i = ε_i * ε₀ / t_i

t_i thickness of insulator

ε₀ permittivity of the air

ε_i permittivity of the insulator material, InP

The charge within the surface depletion region is given by

$$Q_{sc} = -\sqrt{2q N_a \epsilon_s \Psi_s} \quad (14)$$

Total charge in the inversion layer is given by:

$$Q_n(y) = -(Q_s(y) + Q_{sc}(y)) \quad (15)$$

Let dR be the channel resistance of an element section 'dy' is given as

$$dR = \frac{dy}{z \epsilon_n(y) Q_n'(y)} \quad (16)$$

Voltage drop across element section is given by

$$dv = \frac{I_d dy}{z \epsilon_n(y) Q_n'(y)} \quad (17)$$

Drain current at element section 'dy' is given by

$$I_d dy = z \epsilon_n(y) Q_n'(y) dv \quad (18)$$

Integrating from source (y=0, V=0) to the drain (y=1, V=V_d) we get,

$$I_d' \int_0^x dx = z \epsilon_n \int_0^V [V_{gsop} - \Psi_s] C_i + [2q N_a \epsilon_s (\Psi_s)] dv \quad (19)$$

Solving equation 4.24 with Taylor's series,

$$I_d' = \frac{z \epsilon_n C_i}{l} \left\{ (V_{gsop} - \Psi_s - \frac{V_d}{z}) V_d - \left(\frac{t}{z} + \frac{\sqrt{q N_a \epsilon_s / V_{bi}}}{4 C_i} \right) V_d^2 \right\} \quad (20)$$

For smaller values of drain voltages i.e. when V_d < (V_{gsop} - V_t), drain current is given as,

$$I_d' = \frac{z \epsilon_n C_i}{l} (V_{gsop} - V_t) V_d \quad (21)$$

where V_t is the threshold voltage.

The drain voltage when increased to a point, such that the charge in the inversion layer Q(y) at y=1 becomes zero, this point is called as pinch-off point. The drain voltage and drain current at this point designated as V_{dsat} and I_{dsat} respectively. Beyond the pinch-off point it is saturation region.

$$V_{dsat} = V_{gsop} - 2V_{bi} + K^2 \left[1 - \sqrt{1 + \left(\frac{2V_{gsop}}{K^2} \right)} \right] \quad (22)$$

where k = $\frac{\sqrt{2q N_a \epsilon_s (2V_{bi})}}{C_i}$ and

$$I_{dsat} = \frac{z \epsilon_n \epsilon_i}{2t_i l} (V_{gsop} - V_t)^2 \quad (23)$$

Quantum efficiency of the device is calculated using

$$\eta \eta = \frac{I_p h c}{P_0 e \lambda} \quad (24)$$

Computations and simulations have been carried out for InGaAs MISFET at 300K under various illuminated conditions using 3D modeling. The gate metallization has been assumed to be thin enough to allow 90% of the incident radiation to pass through. The parameters used in the calculations are shown in Table1.

Table 1 Parameters used in modeling of the device

Parameter	Values
Channel length, L	0.2 μm

Active layer thickness of MISFET, t_i	390 nm
Channel width, w	100 μm
Reflection coefficient at entrance, metal, insulator, R_s, R_m, R_i	10 % of P_{opt}
Intrinsic doping concentration, n_i	$2.47 \times 10^{17} \text{ m}^{-3}$
Temperature, T	300 K
Drain voltage, V_d	1.5V
Gate voltage, V_{gs}	0.6V
Absorption coefficient, α	$10^6 / \text{cm}$
Wavelength of incident radiation, λ	1.65 μm
Operating frequency, f	1 GHz
Minority Carrier lifetime, τ	10^{-8} s
Straggle Parameter, σ	$0.1 \times 10^{-6} \text{ m}$
Projected Range, R_p	$0.2 \times 10^{-6} \text{ m}$
Position of Fermi level below conduction band, Δ	0.02 eV

V. RESULTS AND DISCUSSION

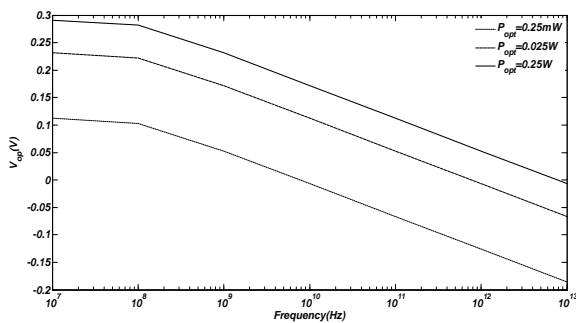


Fig. 2 Variation of photo-voltage with frequency

Fig. 2 shows the graph of photo-voltage versus frequency at constant illumination. The photo-voltage remains constant up to 100 GHz after which the value decreases with increase in signal frequency. This is because the co-efficient associated with the exponential term contributes significantly at a frequency above 100 GHz. The recombination term has very little contribution.

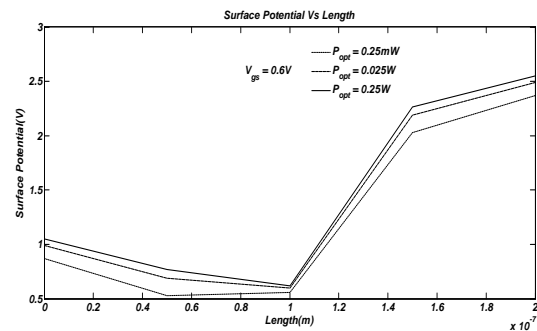


Fig. 3 Variation of Surface Potential with Length for various illumination

Fig. 3 shows the variation of the surface potential along the channel length under illumination ($P_{opt} = 0.25\text{mW}, 0.025\text{W}$ and 0.25W). It can be clearly seen that the channel potential increases with the increase in illumination. This is because with the illumination a forward biasing potential is developed at the gate which increases the surface potential as the illumination increases.

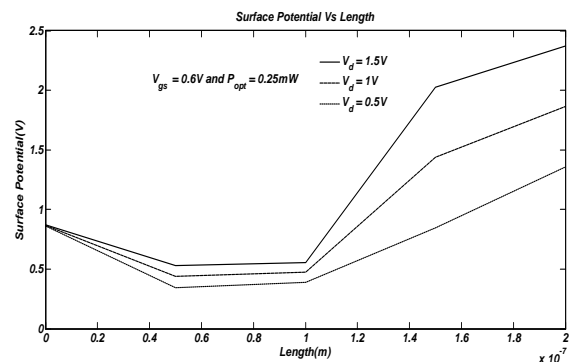


Fig.4 Variation of Surface Potential with Length for various V_d

Fig. 4 shows the variation of surface potential versus length at the illumination of 0.25mW and gate voltage of 0.6V. The curve shows that with increase in V_d the surface potential increases at the drain and the curve shifts upwards on the drain side and there is no change in surface potential at the source side. This is because the potential barrier is increased by the increase in drain bias at the drain side.

Fig. 5 shows the variation of E_y with length for various V_d at the illumination of 0.25mW and gate voltage of 0.6V. The plot shows that field is maximum near drain and also the plot shows that E_y increases with V_d and the effect is prominent near the drain. This is because the biasing potential is applied along Y direction and at the drain.

Fig. 7 shows the variation of E_x with L_x for various V_d . The plot shows that the field is maximum in the depletion region and increases with increase in V_d .

Fig. 8 shows the variation of E_x with L_x for various illumination. It is observed that the change in the field with illumination is more prominent as

compared with E_y because the field E_x and illumination are along same direction. It is also observed that the effect of illumination is prominent near the source as compared to drain. This is because biasing is applied at the drain.

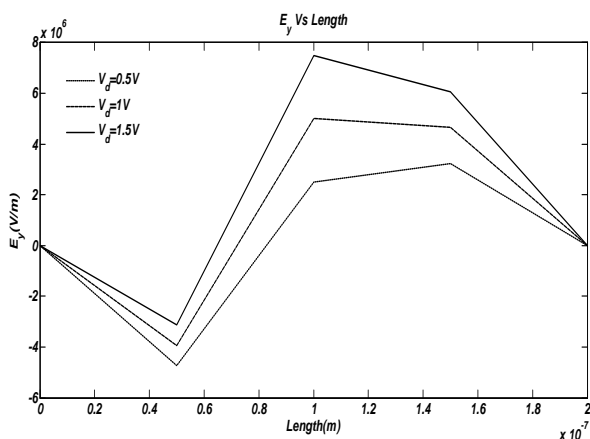


Fig. 5 E_y Vs Length for various V_d

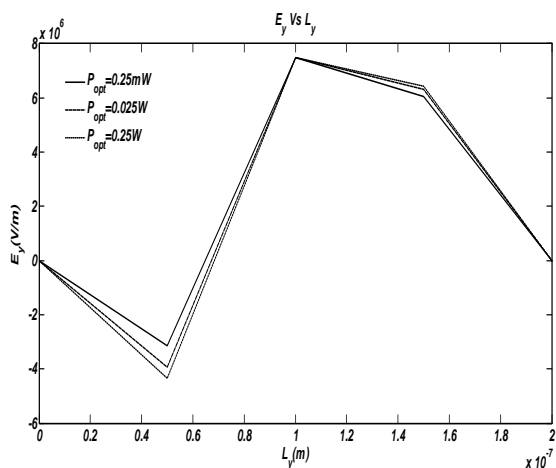


Fig. 6 E_y Vs L_y for various illumination

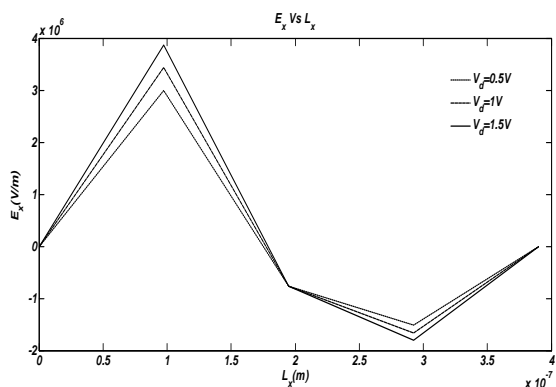


Fig. 7 E_x Vs L_x for various V_d

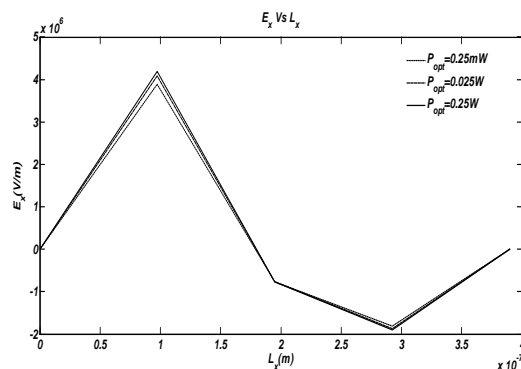


Fig. 8 E_x Vs L_x for various illumination

Fig.9 shows the variation of the drain current with the drain voltage for different gate voltages at the illumination of 0.25mW. It shows that the current increases with increase in gate voltage. The current plot shows good variation in the current as the device enters from linear into saturation with the increase in V_d .

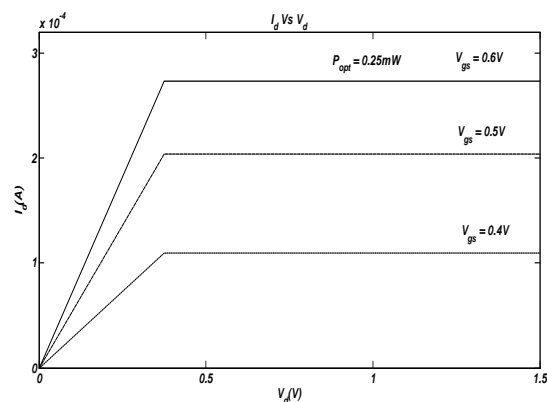


Fig. 9 Drain current Vs drain voltage for various gate voltages

Fig. 5.10 shows the variation of drain current with the drain voltage for various illuminations at the gate voltage of 0.4V. It can be seen that the saturation drain current of the device increases with the increase in illumination. It is also seen that the change in the saturation drain current is significant when incident optical power is large. The saturation drain current in the illuminated condition depends on the surface potential value which changes exponentially with excess photo-generated carriers which in turn increases linearly with the incident optical power. It is thus possible to vary the saturation drain current of the device by using the incident optical power as a controlling parameter and keeping V_g constant. This feature will enable the device to be used as an optically controlled device.

Quantum efficiency of the device is found to be 87% using equation (24) which is better as compared to 60-70% efficiency of InGaAs p-i-n diode [12].

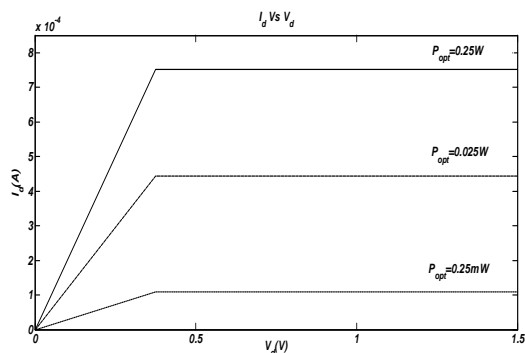


Fig. 10 Drain current Vs drain voltage for various illumination

VI. CONCLUSION

A three-dimensional simulation program for InGaAs has been developed. The program solves numerically the basic continuity equations. The model has been applied to simulate the characteristics under different illuminated conditions. The numerical model developed here computes the various d.c. characteristics, including photo-voltage, variation of gate depletion width in the channel and the current-voltage characteristics. Quantum efficiency of the model represented is better than p-i-n photo-diode. The model presented here can be used to characterize MISFET for optically controlled applications. The results obtained from the simulation are comparable with reported results for similar structures.

References

- [1] Gerd Keiser, "Optical Fiber Communication", Tata McGraw Hill, 4th Edition, 2010.
- [2] John M. Senior, "Optical Fiber Communication", Pearson education limited, 3rd Edition, 2010.
- [3] S. M. Sze, "Semiconductor Devices Physics and Technology", Wiley, 2nd Edition, 2002.
- [4] J. Aiden Higgins, "III-V Technologies: A Growth Industry for 21st Century", GaAs 99-Munich 1999, pp 485-490.
- [5] Y. Kim, M. Dahlstrom, S. Lee, "InP/In_{0.53}Ga_{0.47}As/InP double heterojunction bipolar transistors on GaAs substrates using InP metamorphic buffer layer", *Solid-State Electronics* 46(2002), pp 1541-1544.
- [6] M. S. Alam¹, M. S. Rahman¹, 'Refractive Index, Absorption Coefficient, and Photoelastic Constant: Key Parameters Of InGaAs Material Relevant To InGaAs-Based Device Performance', 2007 International Conference on Indium Phosphide and Related Materials Conference Proceedings 19th IPRM 14 - 18, May 2007 Matsue, Japan.

- [7] Gayatri Phade, Dr B. K. Mishra, "Characterization of Optical MISFET", *International Journal of Engineering Trends and Technology*, Vol. 4, Issue 2, 2013.
- [8] B. K. Mishra, Lochan Jolly, Kalawati Patil, "Modeling and Simulation of 2-D GaAs MESFET under illumination", *International Journal of Recent Trends in Engineering and Technology*, Vol. 4, No. 3, Nov 2010.
- [9] M. Kabeer, K. Gowri, V. Rajamani, "Three Dimensional Modeling and Simulation of a Nano MISFET Photo-Detector", *Journal of Optoelectronics and Advanced Materials*, Vol. 9, No. 9, Sept 2007, pp 2879-2885.
- [10] Shubha, B. B. Pal, R. U. Khan, "Optically controlled Ion-Implanted GaAs MESFET Characteristic with Opaque Gate", *Journal on Electron Devices*, Vol. 45, January 1998, 78-84.
- [11] B.B. Pal and S. N. Chattopadhyay, "GaAs OPFET Characteristics Considering the Effect of Gate Depletion with Modulation Due to Incident Radiation", *Journal on Electron Devices*, Vol. 39, May 1992, pp. 1021-1027.
- [12] Djfar k. Mynbaev, Lowell L. Scheiner, "Fiber Optic Communications Technology", Pearson Education, 4th Edition, 2004.